Supplementary information

Closing the stability-performance gap in organic thermoelectrics by adjusting the partial to integer charge transfer ratio

Osnat Zapata-Arteaga, Bernhard Dörling, Aleksandr Perevedentsev, Jaime Martin, J. Sebastian Reparaz and Mariano Campoy-Quiles

Pictures provided in this file belong to the authors of this work.

Table S1. Summary of organic systems and reported doping mechanisms.

Polymer matrix	dopant	Doping mechanism	Reference (DOI)	Comments
PBTTT	F4TCNQ	both	this work	IR and absorption spectroscopy
	Several	ICT	10.1038/s41586-019-1504-9	IR and absorption spectroscopy
	F4TCNQ	both	10.1021/ma501547h	speculated from absorption experiments
p(g42T-TT)	F4TCNQ	ICT	10.1038/s41563-018-0263-6	IR and absorption spectroscopy
rr P3HT	F4TCNQ	both	this work	IR and absorption spectroscopy
	F4TCNQ	both	10.1021/acs.jpclett.8b03104	IR spectroscopy
	F4TCNQ	both	10.1039/C8MH00223A	IR and absorption spectroscopy
	$FeCl_3$	ICT	10.1038/srep44704	Absorption spectroscopy
	$MoCl_5$	ICT	10.1039/C6TC05544C	Absorption spectroscopy
rra P3HT	F4TCNQ	both	10.1021/acs.jpclett.8b03104	IR
4T		CTC	10.1038/ncomms9560	IR

		CTC	10.1021/cm201798x	DFT (mulliken population)
PDPP(6-DO)2TT	F6TCNNQ		10.1021/acs.macromol.6b02452	Absorption spectroscopy
DBTTTF	Several	both	10.1021/acs.chemmater.8b01447	IR and absorption spectroscopy
PDPP3T	FeCl3	ICT	10.1038/srep44704	Absorption spectroscopy
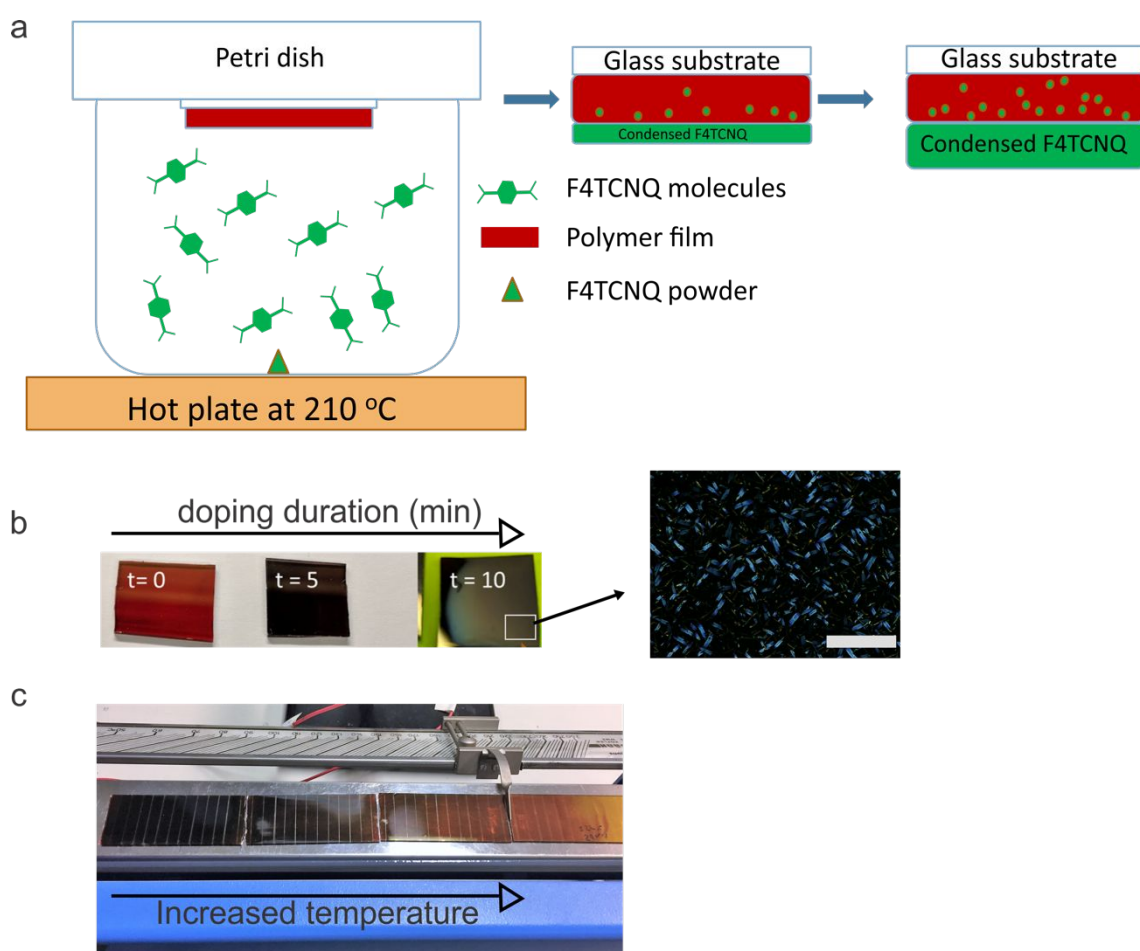
Figure S1. Experimental setup and process used for doping the polymer films and de-doping them under a temperature gradient. a) Dopant is evaporated inside a closed beaker, with the sample attached face-down to the lid. b) Photographs of P3HT with different doping durations. All films doped for longer than 10 minutes yielded surface haziness caused by dopant crystals on the surface, as shown in the inset. In the

micrograph, dopant crystals are visible under polarized light. Scale bar is 100 μm. c) Photograph of films blade coated onto 4 microscope slides, being de-doped in the temperature gradient of a Kofler bench.

For vapor doping, approximately 5 mg of F4TCNQ on the bottom of a 200 mL crystallization beaker was preheated to 210 ºC for 10 min to achieve a sublimation rate of approximately 0.5 μg/s. The sample was attached to a petri dish that served as the lid and holder. For doping gradients, doped films were placed on a preheated Kofler bench for 20 min, using a range of 70 ºC to 220 ºC. De-doped samples were sliced into quasi-homogeneous sections, each measuring 6 mm x 25 mm. Silver paint on the edges served as electrodes.
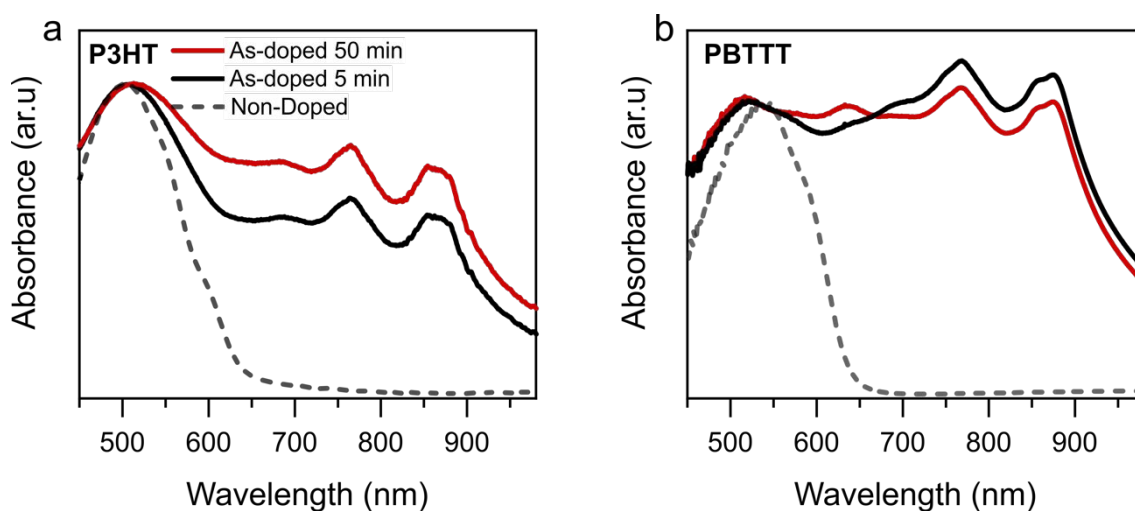
Figure S2. Absorption spectra for a) P3HT and b) PBTTT, for doping durations of 5 and 50 min referred to in the main text as the partially and maximally-doped samples respectively.

Vis-absorption for doped PBTTT shows two bands that correspond to the A⁻ transitions (~ 760 and 890 nm, Figure S2) and a broad band of the P⁺ transition (~ 1500 to 2500 nm, Figure S4). Here, partially-doped samples of P3HT and PBTTT exhibit

essentially identical spectral features. However, maximally-doped samples of PBTTT show an additional weak band emerging around 640 nm (Figure S2b) which, in fact, is *not* seen in the case of P3HT (Figure S2a). We emphasize that this spectral feature does not belong to the NP, A⁻ or P⁺ bands; hence, due to its similarities with other CTCs, we assign it as such.[1,2]
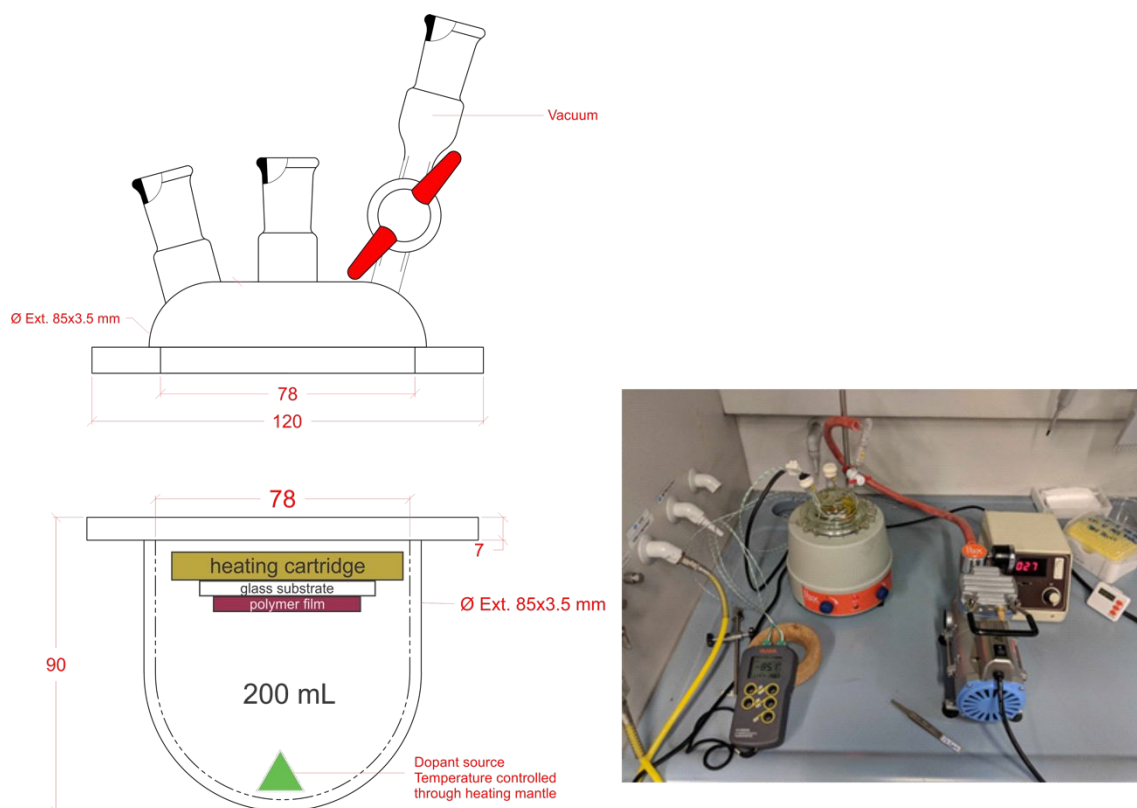
Figure S3. Scheme and photograph of the reactor beaker used as a doping vessel. Thermocouples attached through the 14/24 inlets allowed tracking the temperature of both the polymer substrate and on the bottom of the beaker, where the dopant source is located. Temperature was controlled through a power controller connected to a heating cartridge and the setup was evacuated before beginning.

Alternatively, a few select samples were doped in a 200 mL reactor beaker modified with a heating cartridge and thermocouples as detailed in the experimental section.

Samples were placed on the heating block and doped, varying either duration or temperature.
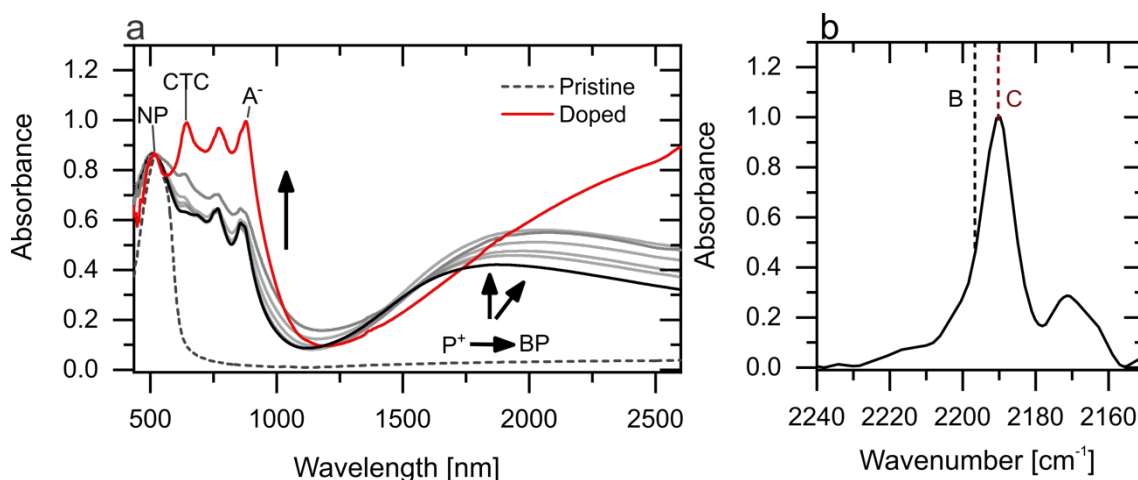

Figure S4. a) Absorption spectra for pristine PBTTT (black dashed line) and doped PBTTT with increasing doping level (from black to red curves). b) IR spectra centered on the -C≡N stretching region for partially doped PBTTT with F4TCNQ. The indicated SC and B (here absent) bands correspond to dopant located close to the backbone and closer to the side chains and backbone respectively.

Figure S5 reveals that the Seebeck coefficient of P3HT decreases from 170 to 100 µV/K within a concurrent change of the electrical conductivity by three orders of magnitude. This is the expected anti-correlation between Seebeck α and σ. On the other hand, α in PBTTT varies from 100 to 48 µV/K with negligible changes in the electrical conductivity, which may suggest that dopant in PBTTT, is more stable to annealing than in P3HT. Alternatively, it can be argued that such changes in α arise from morphological changes during annealing, varying the degree of order and thus, the vibronic contributions that affect the Seebeck coefficient.[3] A final interpretation could be that some of the dopant visible in spectroscopy may not contribute to the electrical conductivity.
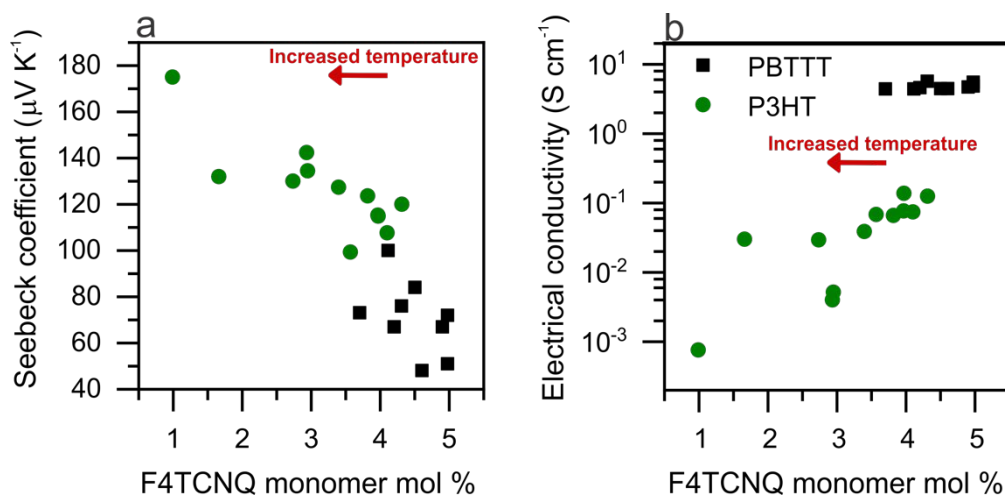
Figure S5. a) Measured Seebeck coefficient and b) electrical conductivity as a function of estimated dopant content. Data belongs to the samples measured in Figure 1 of the main text.

Fitting the spectral features of P3HT and PBTTT shows that, the low and high end of σ correspond to a dopant content of 1 and 4 mol % respectively, while for PBTTT dopant content changes between 3.5 and 5 mol %.
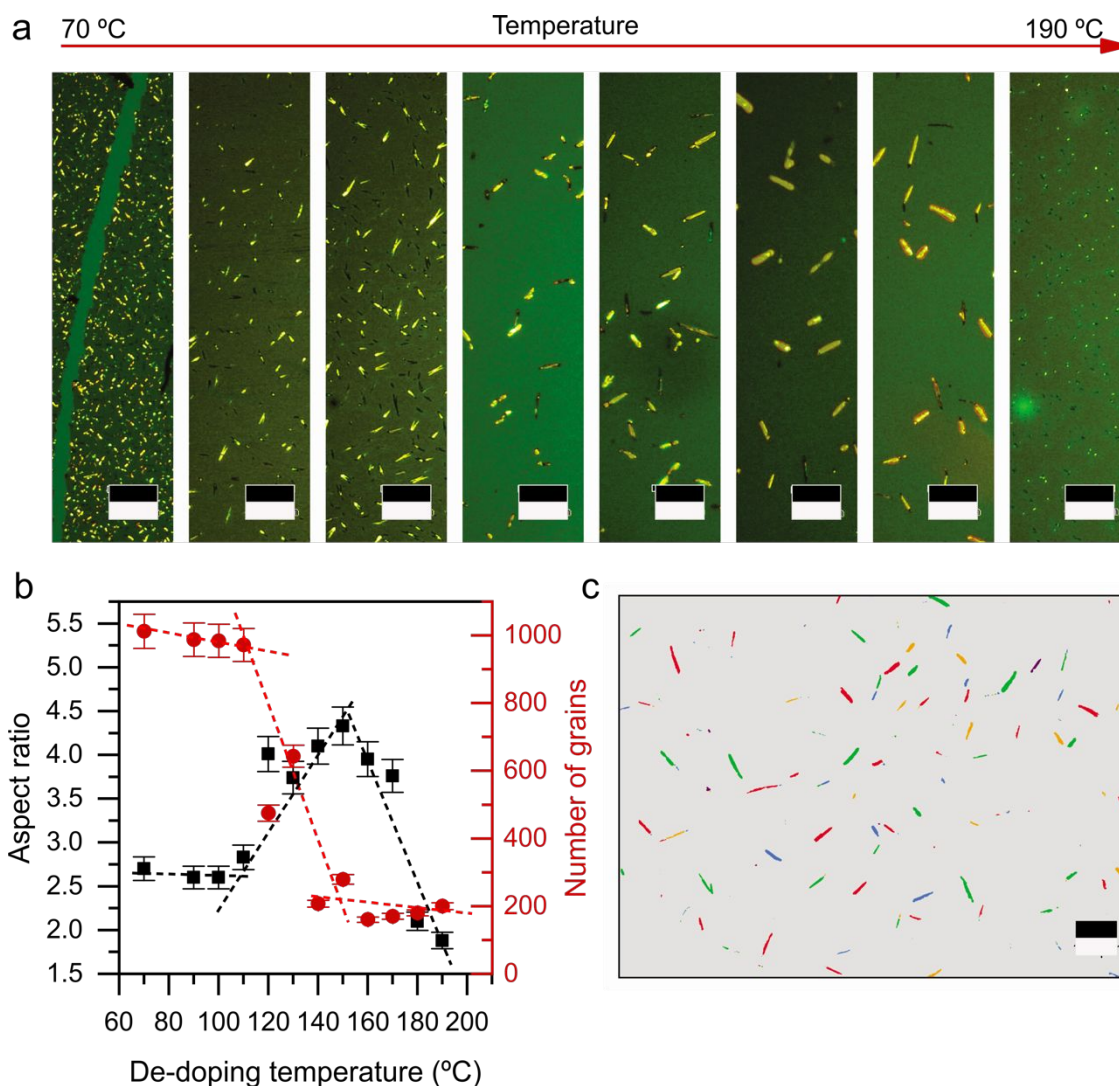
Figure S6. a) Micrographs of a 50-minute doped P3HT film after 20-minutes of de-doping by thermal annealing. Each picture corresponds to a different de-doping temperature. Pictures above 190 ℃ are omitted, scale bar is 100 μm. b) Aspect ratio (black squares) and number of grains (red circles) as a function of de-doping temperature. Dashed lines indicating the change in slope of the estimated behavior seen in the data. c) Example of a micrograph processed with Digital Surf MountainsMap software.

Microscopy

Micrographs of F4TCNQ/PBTTT samples picturing sample regions exposed to different de-doping temperatures (Figure S6a) provide further insight into the de-doping

process. In our experiments, maximally doped samples showed a high density of F4TCNQ crystals on the surface. With this in mind, by tracking the evolution of the number of grains and their aspect ratio as a function of the de-doping temperature (Figure S6b) we infer three regimes. (1) For 100–120 °C, non-active and de-doped F4TCNQ migrates to the surface, resulting in further growth of the surface crystals due to continuous expulsion of F4TCNQ from the polymer film as well as Ostwald ripening, as evident from the increased aspect ratio and reduced number of crystals. (2) A change in the slope beyond 140 °C suggests a competition between the sublimation of surface crystals and the above-described growth. (3) Finally, above 170 °C sublimation most likely dominates. Elsewhere, de-doping experiments on F4TCNQ/P3HT have shown that dopant diffuses out of the polymer backbone region at a lower temperature (60–80 °C) than from the side chains (80–120 °C).[4] In our case, micrographs show little to no change below 100 °C, which agrees with the absent B band in the IR spectra (Fig S4b) (i.e. no dopant in the backbone or near the backbone).

Table S2. Electrical conductivity of PBTTT doped using different substrate temperatures (T_{sub}) with a doping time t_d

| Conditions T_{sub}/t_d	Electrical conductivity [S cm^{-1}]
70 °C / 10 min	8.6
90 °C / 10 min	24.8
110 °C / 10 min	30.9
130 °C / 10 min	85.1
150 °C / 10 min	52.3
190 °C / 10 min	28.0
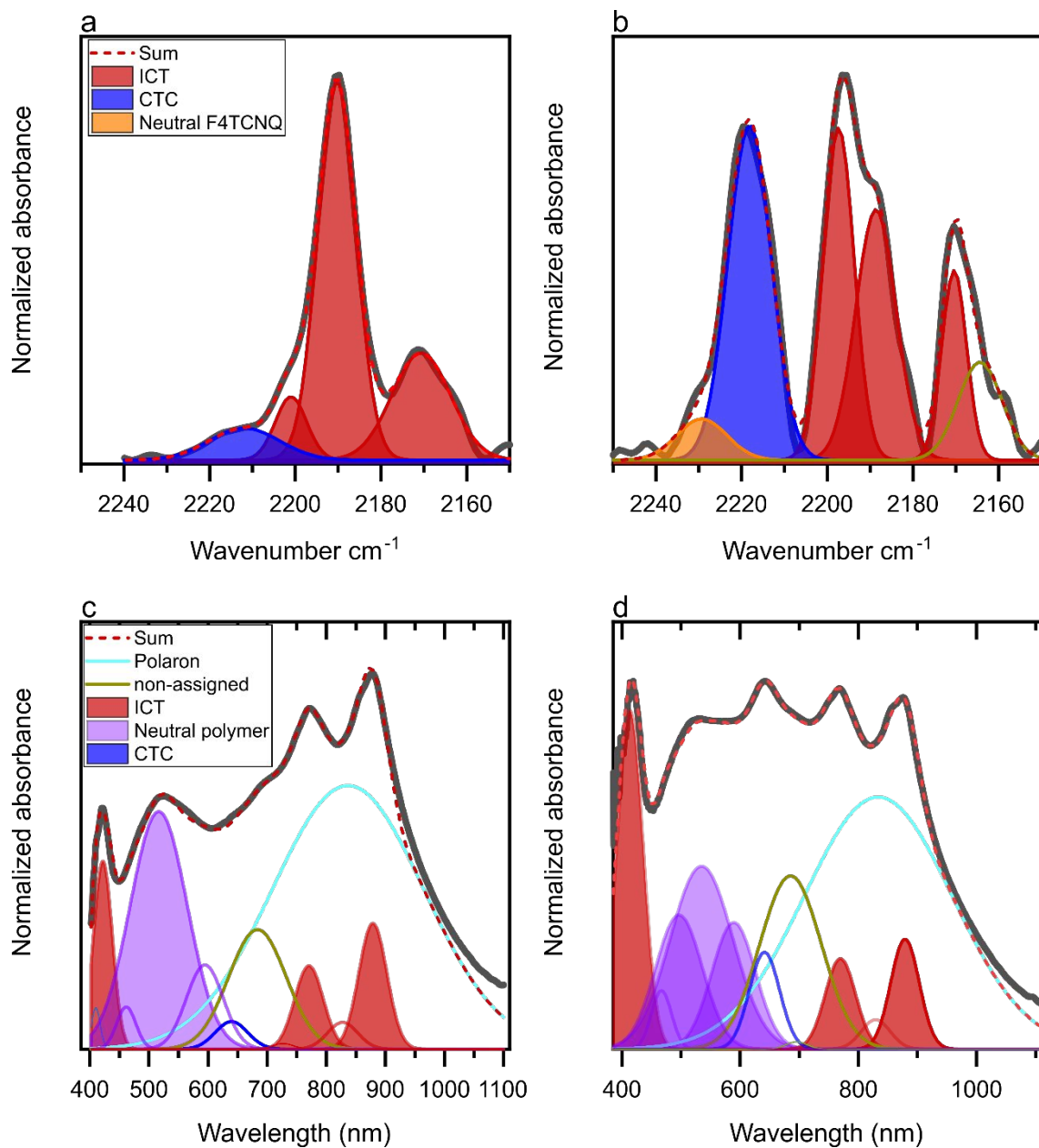
Figure S7. IR spectra of selected samples. Here, we show doped PBTTT with (a) low χ_{CTC} content and (b) with a moderate χ_{CTC} content. Corresponding absorption spectra of the same samples, are shown for c) low and d) moderate χ_{CTC} scenarios. Spectra were subjected to peak fitting and the integrated intensity was used to estimate the dopant content and the CTC fraction.

A precise value for the CTC fraction of the *low* χ_{CTC} samples is not given, due to the low intensity and similarities of the assigned CTC peak and the neutral polymer aggregates reported in literature.[5] Yet, as seen in the IR spectra for the same sample (Figure S7 a) it is possible to introduce the same CTC band seen for the samples with a higher CTC content. This agrees with the coexistence of different charge-transfer states in highly doped polymers seen by Neelamraju et al. [6] On the other hand, samples with a *maximum* χ_{CTC} content show no visible neutral polymer or anion features, which makes spectral fitting highly unreliable.

Quantifying the dopant content is possible up to some extent. A common method (1) relies on using the integrated intensity of the A^- and NP features, Beer Lambert's law, and a known attenuation coefficient. While other methods (2) utilize the intensity ratio of the NP band and the isolated polaron features (P^+)[7,8] (seen in Figure S4). Yet, both methods have some uncertainty, since CTC features overlap with the absorption of the A^- and the NP, while the hidden polaron feature (~790 nm) can change in intensity (and thus that of the anion) due to the $P^+ \rightarrow BP$ formation with increased dopant content. Alternatively, using the isolated P^+ features introduce error, since both the center and shape change gradually with doping level.
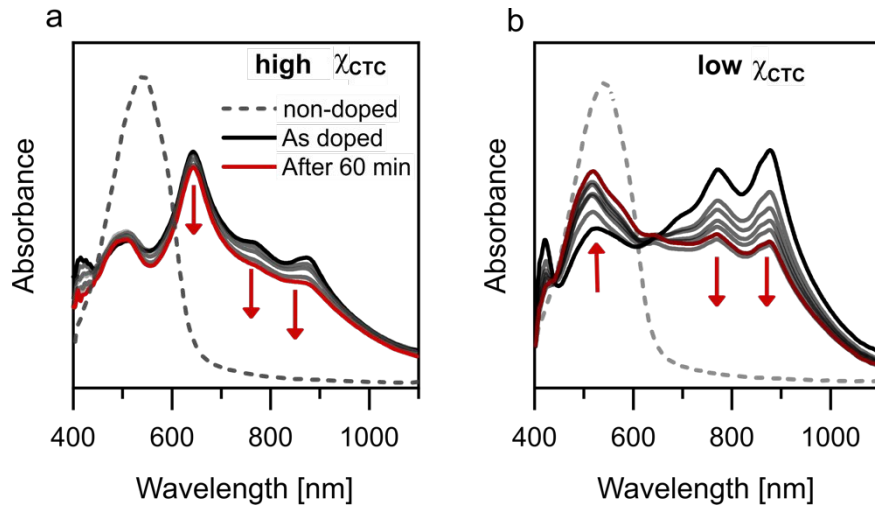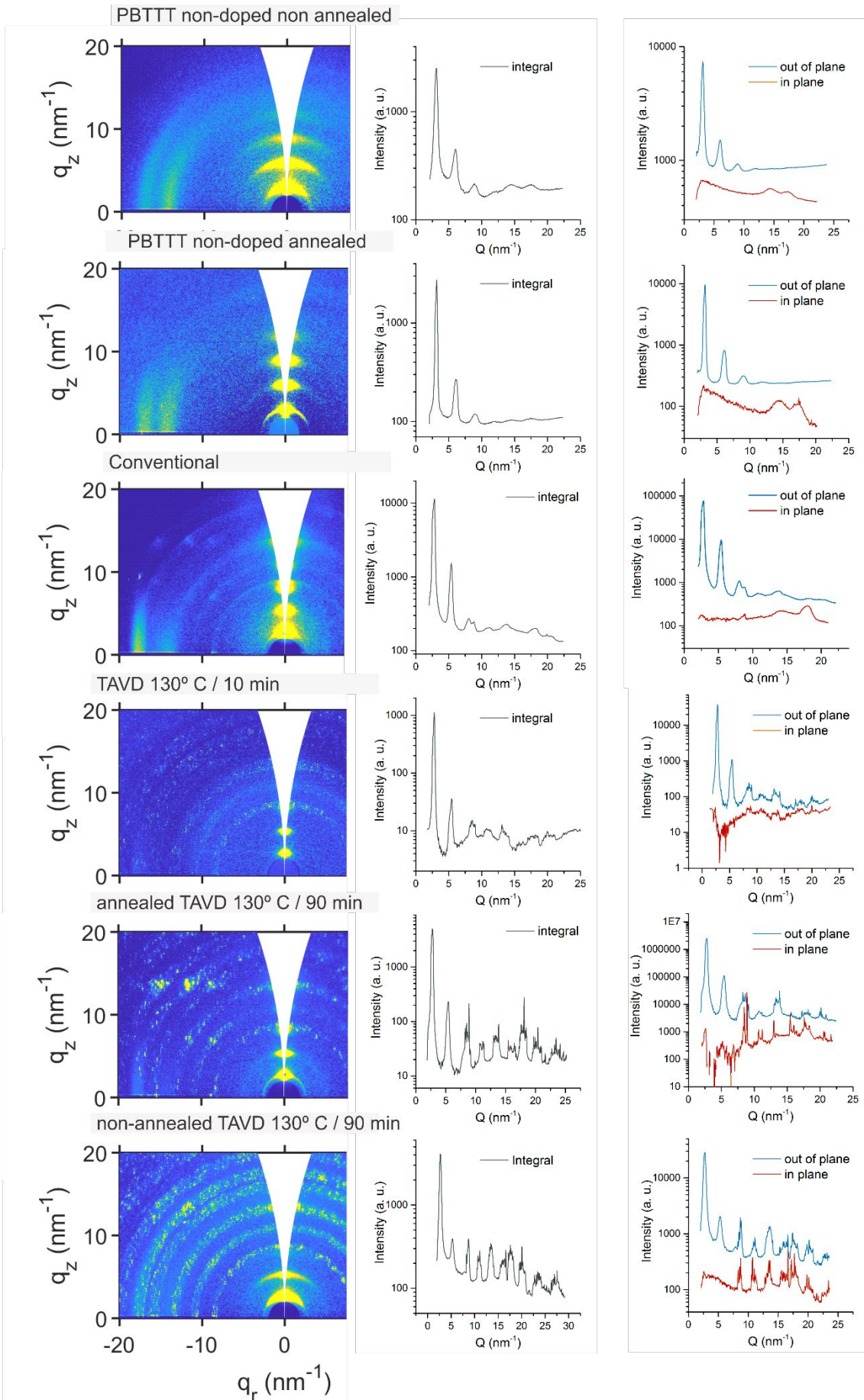
Figure S8. Absorption spectra of PBTTT doped with F4TCNQ. Series in this experiment contain (a) high and (b) low χ_{CTC}. The black curve shows the as-doped samples which progress with time (arrow direction) towards the red curves (after 60 min of annealing). Dashed lines show the pristine material (non-doped) and grayscale curves show the spectra at in-between t_{dd}. Data is normalized by film thickness (~230nm) due to the nearly bleached NP transition in samples with high χ_{CTC}.
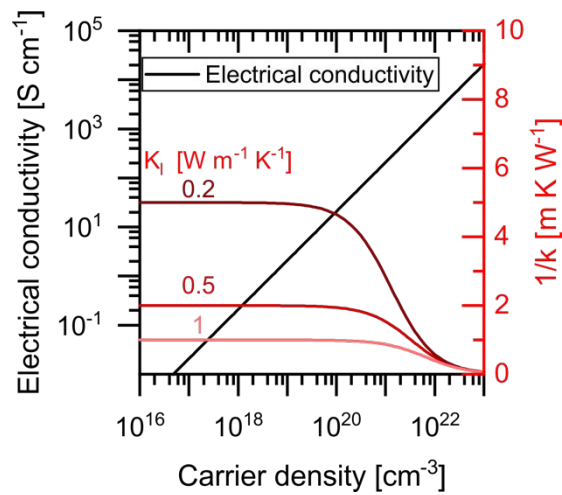
Figure S9. Estimated electrical conductivity (black curve) and total thermal conductivity (red scale curves) as a function of carrier density. Thermal conductivity is estimated with different $\kappa_{lattice}$.

Total thermal conductivity (κ_{total}) is estimated as the contribution from the lattice ($\kappa_{lattice}$) and electronic ($\kappa_{electron}$) thermal components ($\kappa_{total} = \kappa_{electron} + \kappa_{lattice}$). Electronic contribution is calculated with the Wiedemann-Franz law, using the Sommerfeld value for a degenerate Fermi gas as the Lorentz factor (L). Electrical conductivity is calculated using the electron mobility commonly reported for PBTTT (1 cm^2/V·s)[9]. As we can see here, only for values of σ above 100 S cm^{-1} does the electronic contribution to κ_{total} become important. Below that value, the total thermal conductivity is nearly identical to the $\kappa_{lattice}$ contribution.

PBTTT non-doped non annealed

PBTTT non-doped annealed

Conventional

TAVD 130° C / 10 min

annealed TAVD 130° C / 90 min

non-annealed TAVD 130° C / 90 min

Figure S10. GIWAXS patterns with selected processing conditions and integrated data of the in-plane and out-of-plane intensities. Here, conventional refers to the non-heated substrate conditions.

(1)   Méndez, H.; Heimel, G.; Winkler, S.; Frisch, J.; Opitz, A.; Sauer, K.; Wegner, B.; Oehzelt, M.; Röthel, C.; Duhm, S.; et al. Charge-Transfer Crystallites as Molecular Electrical Dopants. *Nat. Commun.* **2015**, *6*, 8560.

(2)   Jacobs, I. E.; Cendra, C.; Harrelson, T. F.; Bedolla Valdez, Z. I.; Faller, R.; Salleo, A.; Moulé, A. J. Polymorphism Controls the Degree of Charge Transfer in a Molecularly Doped Semiconducting Polymer. *Mater. Horizons* **2018**, *5* (4), 655–660.

(3)   Venkateshvaran, D.; Nikolka, M.; Sadhanala, A.; Lemaur, V.; Zelazny, M.; Kepa, M.; Hurhangee, M.; Kronemeijer, A. J.; Pecunia, V.; Nasrallah, I.; et al. Approaching Disorder-Free Transport in High-Mobility Conjugated Polymers. *Nature* **2014**, *515* (7527), 384–388.

(4)   Hase, H.; O'Neill, K.; Frisch, J.; Opitz, A.; Koch, N.; Salzmann, I. Unraveling the Microstructure of Molecularly Doped Poly(3-Hexylthiophene) by Thermally Induced Dedoping. *J. Phys. Chem. C* **2018**, *122* (45), 25893–25899.

(5)   Wang, C.; Duong, D. T.; Vandewal, K.; Rivnay, J.; Salleo, A. Optical Measurement of Doping Efficiency in Poly(3-Hexylthiophene) Solutions and Thin Films. *Phys. Rev. B* **2015**, *91* (8), 085205.

(6)   Neelamraju, B.; Watts, K. E.; Pemberton, J. E.; Ratcliff, E. L. Correlation of Coexistent Charge Transfer States in F 4 TCNQ-Doped P3HT with Microstructure. *J. Phys. Chem. Lett.* **2018**, *9* (23), 6871–6877.

(7)   Jacobs, I. E.; Aasen, E. W.; Oliveira, J. L.; Fonseca, T. N.; Roehling, J. D.; Li, J.; Zhang, G.; Augustine, M. P.; Mascal, M.; Moulé, A. J. Comparison of Solution-Mixed and Sequentially Processed P3HT:F4TCNQ Films: Effect of Doping-Induced Aggregation on Film Morphology. *J. Mater. Chem. C* **2016**, *4* (16), 3454–3466.

(8)   Lim, E.; Peterson, K. A.; Su, G. M.; Chabinyc, M. L. Thermoelectric Properties of Poly(3-Hexylthiophene) (P3HT) Doped with 2,3,5,6-Tetrafluoro-7,7,8,8-Tetracyanoquinodimethane (F 4 TCNQ) by Vapor-Phase Infiltration. *Chem. Mater.* **2018**, *30* (3), 998–1010.

(9)   Brocorens, P.; Van Vooren, A.; Chabinyc, M. L.; Toney, M. F.; Shkunov, M.; Heeney, M.; McCulloch, I.; Cornil, J.; Lazzaroni, R. Solid-State Supramolecular Organization of Polythiophene Chains Containing Thienothiophene Units. *Adv. Mater.* **2009**, *21* (10–11), 1193–1198.